COBEM 2021 26th International Congress of Mechanical Engineering
November 22-26, 2021, Virtual Congress, Brazil

COB2021-0403
NUMERICAL ANALYSIS OF MIXED CONVECTION IN A RECTANGULAR CAVITY AT DIFFERENT ASPECT RATIOS

Roberto Bittar Bigonha[1]
Adriano Possebon Rosa[2]
Department of Mechanical Engineering, Faculty of Technology, University of Brasilia
[1]rb.bigonha@gmail.com
[2]possebon.adriano@gmail.com

Abstract. *Mixed convection occurs when the mechanisms of both natural and forced convection have significant influence on the behavior of the flow and on the resulting heat transfer. The contribution of each motion depends on factors such as temperature gradient, type of flow, external source of movement and geometry. One largely known application for this kind of heat transfer is the cooling of electronic components using air. We analyze, in this work, the effects of mixed convection in a rectangular closed cavity filled with air. We investigate the influence of the aspect ratio on local and average Nusselt numbers for two situations, namely the assisting flow - when forced convection and natural convection go the same way - and the opposing flow - when forced and natural convection go in opposing ways. The left wall is kept at a constant high temperature and the right wall is kept at a fixed low temperature, while the lid and the bottom walls are both adiabatic. The lid is maintained at constant velocity, going right in the case of assisting flow and left in the case of opposing flow. Combinations of Reynolds and Grashof numbers are analyzed. A dimensionless parameter, the Richardson number (defined as the ratio between Grashof and Reynolds squared), is used to express which kind of convection is predominant. If the Richardson number is of order unity, both types are important; If it is much smaller than one, natural convection is unimportant; and if it is much greater than one, forced convection is unimportant. We take the fluid as incompressible and we restrain our investigation to the laminar flows. The governing equations are the Navier-Stokes equations with Boussinesq approximation and the energy equation. A first order projection method with a staggered grid was used to solve the governing equations. The results, analyzed at steady state, show that the local Nusselt number increases with the aspect ratio for both assisting and opposing flows. Plots of temperature and velocity profiles end the paper and help to elucidate the physics governing this category of fluid motion.*

Keywords: *Numerical heat transfer, mixed convection, rectangular cavity, projection method.*

1. INTRODUCTION

Natural or free convection can be defined as the form of heat transfer in which the flow occurs as a result of buoyancy forces in the presence of gravity and density variations between fluid layers. Forced convection depends on the presence of an additional mechanism which is responsible for driving the flow. Mixed convection is characterized by the combination of mechanisms of both these types of convection. Heat transfer by mixed convection is considered significant when forced convection at low speed occurs – that is, when natural convection is non-negligible. This type of process can be seen in the cooling electronic devices or in drying technologies (Oztop and Dagtekin, 2004). The presence of both a shear force and a buoyancy force adds some complexity to the flow. For this reason, the phenomena involving mixed convection inside a cavity have been extensively analyzed in the literature by several different authors in many diverse cases.

Mixed convection can be divided into three types of flow (Çengel and Ghajar, 2015): assisting flow, when the mechanisms of forced convection act in the same direction as those of natural convection; opposing flow, when these mechanisms act in opposite directions; and transverse flow, when the mechanisms of natural and forced convection are perpendicular to each other.

Ameziani *et al.* (2010) studied a square cavity with a horizontal temperature gradient and a moving lid, analyzing the variation on the Nusselt number for various Reynolds and Rayleigh numbers. The results were compared to scale analysis based on the dominant forces and show that for opposing flow there is a value of *Ra* for which *Nu* is minimum.

Cheng and Liu (2010) analyzed the lid-driven cavity with temperature gradients in different directions, namely, upward, downward, leftward and rightward. The results show that the heat transfer rate increases when *Ri* decreases regardless of the orientation of temperature gradient. A better heat transfer rate was obtained for the downward temperature gradient than the upper temperature gradient. This was due to increased buoyancy effects in the lower portions of the cavity.

The publications found in the literature are mostly related to cavities with vertical temperature gradients and restricted

to square cavities. This work consists on the study of mixed convection in a rectangular cavity filled with air at different aspect ratios (*AR*) and various Reynolds and Richardson numbers. This way, it is possible to notice the transition of the dominant form of convection from one to the other. Assisting and opposing flows are observed. The left wall of the cavity is kept at a constant hot temperature, and the right wall is kept at a constant low temperature. The top and bottom walls are adiabatic. The lid moves in the horizontal direction at a constant speed, U_0. On assisting flow, the lid moves right; on opposing flow, it goes left. Figure 1 shows an illustration of the problem.

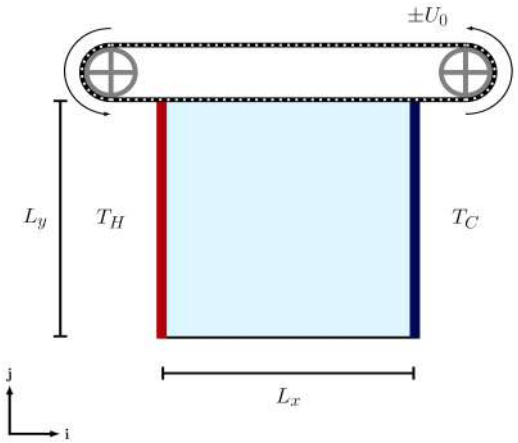

Figure 1: Illustration of the problem.

2. METHODOLOGY

The flow is considered incompressible and the governing equations are the Navier-Stokes equations and the energy equation. The Navier-Stokes equations are used with the Boussinesq approximation so that variations in density are considered only in the buoyancy terms. The equations are given by

$$\nabla \cdot \mathbf{u} = 0, \tag{1}$$

$$\frac{\partial \mathbf{u}}{\partial t} + \mathbf{u} \cdot \nabla \mathbf{u} = -\frac{1}{\rho}\nabla p + \nu \nabla^2 \mathbf{u} + g\beta(T - T_C)\hat{\mathbf{e}}_y \quad \text{and} \tag{2}$$

$$\frac{\partial T}{\partial t} + \mathbf{u} \cdot \nabla T = \alpha \nabla^2 T. \tag{3}$$

The variables ρ and α are the density and the thermal diffusivity. Considering an x, y co-ordinate system at the lower left corner of the cavity, $\mathbf{u}$ is the velocity field, p is the pressure, g is the acceleration of gravity – directed downward –, β is the volume thermal expansion coefficient and ν is the kinematic viscosity. T is the temperature, T_C is the cold temperature at which the right wall is maintained and t is the time. The equations are discretized using finite difference approximations solved by an explicit first order projection method based on the one proposed by Chorin (1968). The non-dimensional forms of the variables are

$$x^* = x/L_x; \qquad y^* = y/L_y; \qquad \mathbf{u}^* = \frac{L\mathbf{u}}{\alpha};$$

$$t^* = \frac{\alpha t}{L^2}; \qquad p^* = \frac{L^2 p}{\rho \alpha}; \qquad \text{and} \qquad \theta = \frac{T - T_C}{T_H - T_C}.$$

L_x is the length of the cavity, L_y is its height, T_H is the hot temperature at which the left wall is maintained and θ, x^* and y^* are the dimensionless temperature, length and height. The non-dimensional groups are defined as

$$Pr = \frac{\mu c}{k}; \qquad Re = \frac{\rho U_0 L_x}{\mu}; \qquad Gr = \frac{\beta g (T_H - T_C) L^3}{\nu^2};$$

$$Ra = Gr\ Pr; \qquad \text{and} \qquad Ri = \frac{Gr}{Re^2},$$

where Pr is the Prandtl number; Re is the Reynolds number; Ri is the Richardson number; Gr is the Grashof number.

The dynamic viscosity is represented by μ, the specific heat is c and the thermal conductivity is k. U_0 is a reference velocity.

The governing equations are solved numerically using a first order projection method in a staggered grid using a finite difference approximation by the following steps:

$$\frac{\mathbf{u}^* - \mathbf{u}^k}{\Delta t} + \mathbf{u}^k \cdot \nabla \mathbf{u}^k = \frac{1}{Re}\nabla^2 \mathbf{u}^k + Ri\ \theta^k, \tag{4}$$

$$\nabla^2 p^{k+1} = \frac{1}{\Delta t}\nabla \cdot \mathbf{u}^*, \tag{5}$$

$$u^{k+1} = \mathbf{u}^* - \Delta t \nabla p^{k+1}, \tag{6}$$

$$\frac{\theta^{k+1} - \theta^k}{\Delta t} + \mathbf{u}^k \cdot \nabla \theta^k = \frac{1}{Re\ Pr}\nabla^2 \theta^k. \tag{7}$$

To implement this algorithm we developed a software in *Python 3* in a 200×200 mesh using *Numba* compiler. The fluid inside the cavity is air ($Pr = 0,71$). In order to avoid numerical instability, restrictions regarding the time step and the spacial increment must be respected, so that

$$\Delta x < \frac{1}{\sqrt{Re}}, \tag{8}$$

$$\Delta t < \Delta x, \tag{9}$$

$$\Delta t < \frac{1}{4} Re \Delta x^2. \tag{10}$$

For every flow, the local Nusselt number at the hot wall is calculated as a measure of heat exchange. The local Nusselt number, Nu_L, can be calculated at each point over the left wall and is given by

$$Nu_L = -\frac{\partial \theta}{\partial x^*}. \tag{11}$$

The average Nusselt number, Nu_{avg}, is obtained integrating Nu_L along the hot wall and is given by

$$Nu_{avg} = -\int_0^1 \frac{\partial \theta}{\partial x^*} dy^*, \tag{12}$$

where Nu_L is the local Nusselt number and Nu_{avg} is the average Nusselt number.

3. RESULTS

All the results presented converge in time through a steady-state.

3.1 Validation

Our code was validated based on the results of the lid-driven cavity obtained by Ghia *et al.* (1982) and the results of pure free convection obtained in four different papers (Barakos *et al.*, 1994; Fusegi *et al.*, 1991; Markatos and Pericleous, 1984; de Vahl Davis, 1983) for different Rayleigh numbers. A 200×200 mesh was used for validation.

Figure 2 shows the result of the validation for the lid-driven cavity. Velocity component u was observed in different points through a vertical line passing through the geometric center of the cavity. For v, a horizontal line passing through the geometric center of the cavity was observed. Both plots show good agreement between the code and the literature for the lid-driven cavity for Reynolds numbers of 100, 400 and 1000.

For pure free convection, the Nusselt number was obtained for Rayleigh numbers of 10^3, 10^4 and 10^5, as shown in Tab. 1. Again, our results agree very well with those of other authors.

Table 1: Nusselt numbers calculated for three distincts values of Rayleigh in four different papers.

Rayleigh	Present Work	Barakos *et al.* (1994)	Fusegi *et al.* (1991)	Markatos and Pericleous (1984)	de Vahl Davis (1983)
10^3	1.116	1.114	1.105	1.108	1.118
10^4	2.239	2.245	2.302	2.201	2.243
10^5	4.511	4.510	4.646	4.430	4.519

A grid refinement study was made to choose the appropriate mesh resolution. The average Nusselt number was analyzed for $Re = 100$ and $Ri = 1$ on assisting flow for several meshes. Mesh distributions ranging from 20×20 to 200×200 were tested. Figure 4 shows that a mesh of 200×200 or finer is fit for grid independent solution. Thus, this configuration was used to ensure low error.

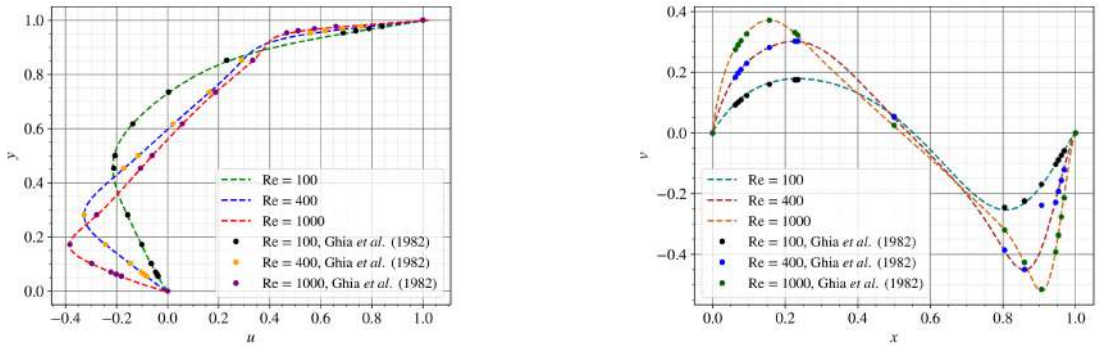

(a) u velocity. (b) v velocity.

Figure 2: Validation for the lid-driven cavity.

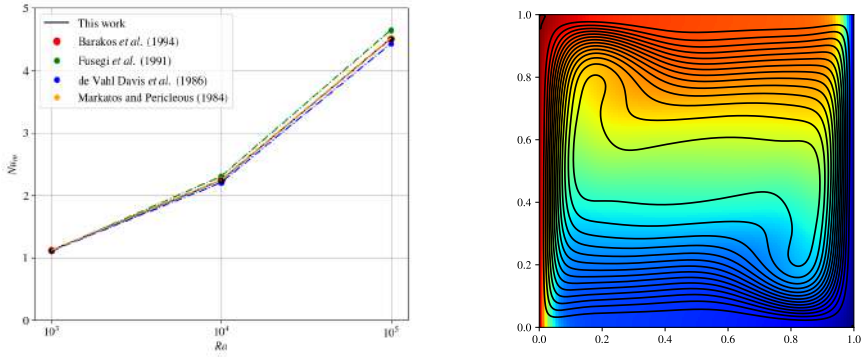

(a) (b)

Figure 3: Validation for the natural convection with Nusselt numbers found in different papers (a) and streamlines with temperature profile for $Re = 10^6$ (b).

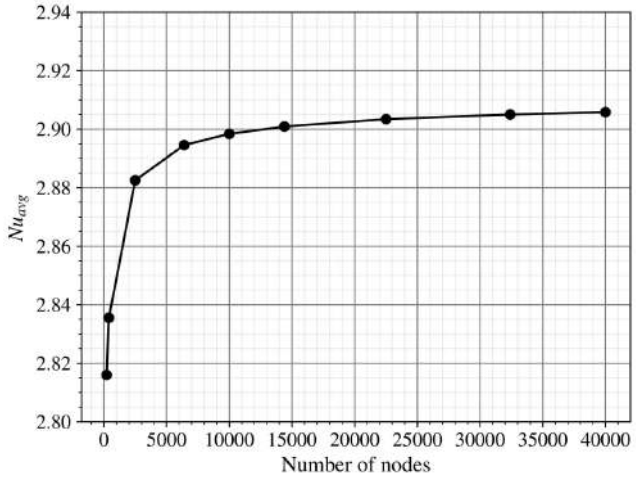

Figure 4: Values of Nu_{avg} for different node numbers.

3.2 Mixed convection

Figure 5 shows the results for $Re = 100$ and $Ri = 1$. In this case, buoyancy and shear forces are balanced and moderate. The streamlines show that for opposing flow, the cavity is clearly divided in a top part – where shear forces are dominant – and a bottom part – where buoyancy forces prevail. The two parts have roughly the same dimension for $AR = 1$. For aspect ratios higher than one, both circulation regions remain visible, but now buoyancy forces tend to take up more space. In these situations, both assisting and opposing flows show similar temperature profiles.

With an increase on the Richardson number, Fig. 6 shows clearly that shear forces start to become less important at

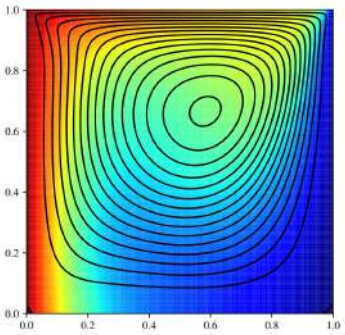

(a) Assisting flow (*AR* = 1).

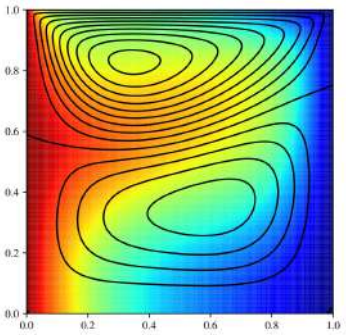

(b) Opposing flow (*AR* = 1).

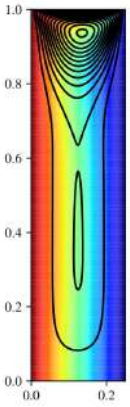

(c) Assisting flow (*AR* = 4).

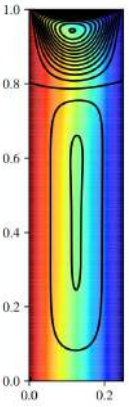

(d) Opposing flow (*AR* = 4).

Figure 5: $Re = 100$, $Ri = 1$.

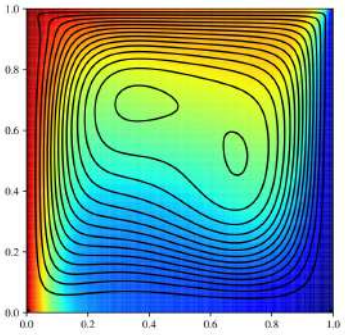

(a) Assisting flow (*AR* = 1).

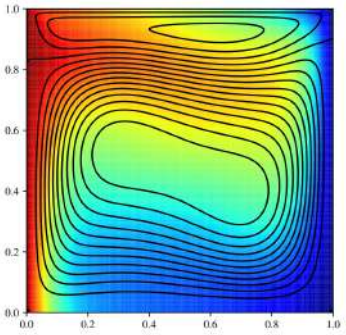

(b) Opposing flow (*AR* = 1).

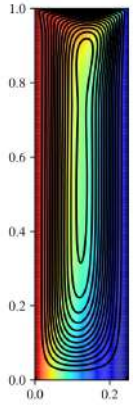

(c) Assisting flow (*AR* = 4).

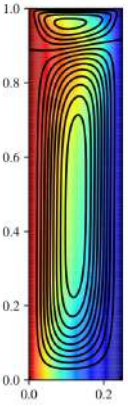

(d) Opposing flow (*AR* = 4).

Figure 6: $Re = 100$, $Ri = 10$.

$Re = 100$ and $Ri = 10$, since the region affected by the motion of the lid is significantly smaller. For AR = 1, the assisting flow behaves similarly to that of natural convection. The opposing flow shows that the effects of shear forces are limited to a small portion on the top part of the cavity. However, they are still visible even for high aspect ratios, with a well defined circulation region due to the movement of the lid.

Figures 7a and 7b show the results obtained for an increased Reynolds number at a fixed Grashof number, with $Re = 1000$ and $Ri = 0.1$ with $AR = 1$. The effects of shear forces are largely dominant for the square cavity in this case. The streamlines for assisting and opposing flows display a symmetrical behavior, with classical signs of the pure lid-driven cavity, such as a central primary vortex and secondary eddies on the bottom corners. Higher aspect ratios start to favor buoyancy effects, as seen in Fig. 7c and 7d. A small eddy on the right wall appears between the two regions on the assisting flow, resulting in a decrease in size of the main eddies.

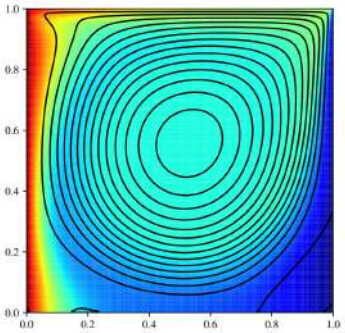

(a) Assisting flow (*AR* = 1).

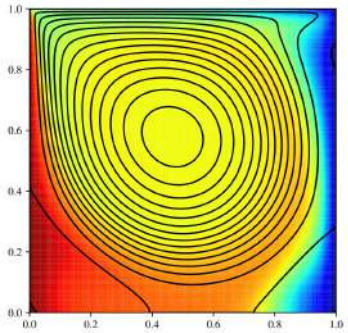

(b) Opposing flow (*AR* = 1).

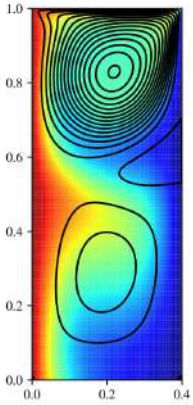

(c) Assisting flow (*AR* = 2.5).

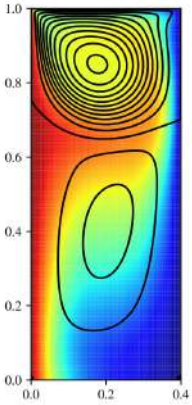

(d) Opposing flow (*AR* = 2.5).

Figure 7: $Re = 1000$, $Ri = 0.1$.

Figure 8a shows what happens when we increase the Richardson number, resulting in $Re = 1000$ and $Ri = 1$. This means that buoyancy forces are expected to play a bigger role, with a strong conflict between the two convection mechanisms along the entire cavity for both assisting and opposing flows. A decentralization of the primary vortex due to a strong combination of buoyancy and shear forces can be seen. The opposing flow for a square cavity, Fig. 8b shows that even though the shear forces are limited to the top part of the cavity, a secondary eddy starts to take form there. The lower part of the cavity shows a great interaction of the two mechanisms involved. For a rectangular cavity, higher aspect ratios showed a regular clockwise flow for aided convection, and in opposing flow the upper part did not undergo major changes in its form when compared to the flow in the cavity with $AR = 1$ in Fig. 8b.

The velocity profiles in Figs. 9 and 10 show that for $Re = 100$ and $Ri = 0.1$, the thermal convection is seen not to play a significant role. A symmetric behavior for assisting and opposing flows can be seen. This shows that, as expected, the flow is driven by shear forces. In this case, the Grashof number is 10^3, which is within the conduction limit. Therefore, convection is insignificant. Similarly, for $Re = 1000$ and $Ri = 0.1$, a symmetrical behavior is seen when observing the velocity profiles for $AR = 1$, showing that for values of Ri lower than unity and $AR = 1$, buoyancy forces tend to be secondary.

Results for $Ri = 1$ and $Ri = 10$ with $AR = 1$ on the other hand showed asymmetrical velocity profiles with clearly visible differences between assisting and opposing cases, suggesting that for this range of Ri a balance between the mechanisms of convection can be observed.

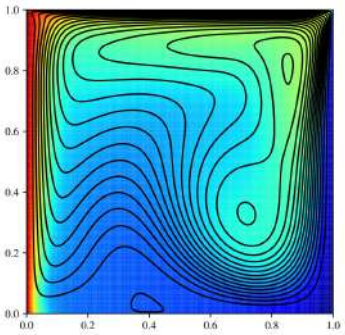

(a) Assisting flow ($AR = 1$).

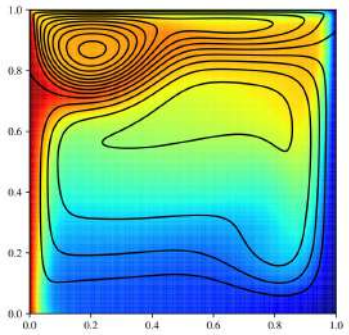

(b) Opposing flow ($AR = 1$).

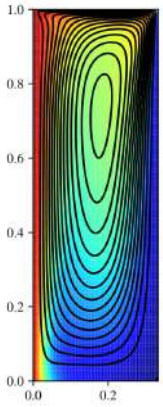

(c) Assisting flow ($AR = 3$).

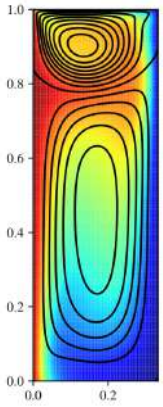

(d) Opposing flow ($AR = 3$).

Figure 8: $Re = 1000$, $Ri = 1$.

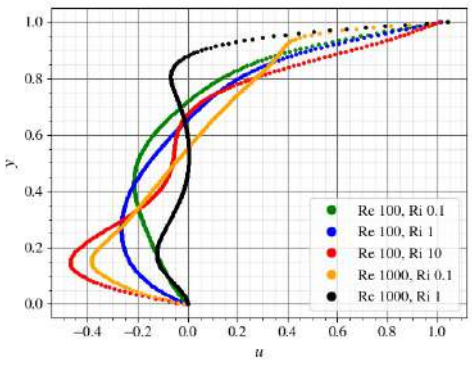

(a) Assisting flow.

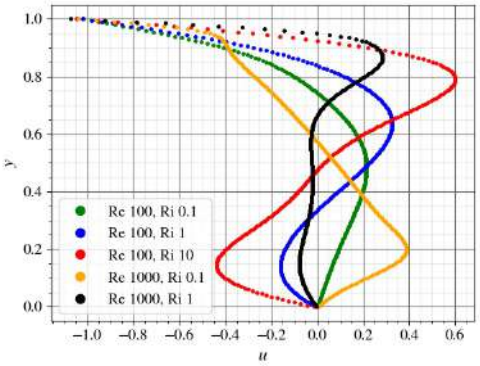

(b) Opposing flow.

Figure 9: u-velocity through a vertical line passing through the geometric center: $AR = 1$.

3.3 Nusselt number

The values of Nu_{avg} were calculated for different combinations of the governing parameters for both assisting and opposing flows. Such values are presented in Fig. 11. On the average Nusselt number, there are not noticed many changes between the opposing and assisting flows at different aspect ratios, except for the case of $Re = 1000$, $Ri = 1$ – probably due to a high Reynolds number and low buoyancy effects. This shows that even though the streamlines go through many changes from one case to the other, heat transfer is not really affected by the direction of the shear forces at moderate values of Ri.

An increasing predominance of the buoyancy forces is observed as the aspect ratio is raised. This can be seen on the streamline plots and on the average Nusselt number, and is an expected result, since the source of the shear forces is limited to the lid of the cavity, while the buoyancy forces have their source distributed along the vertical wall.

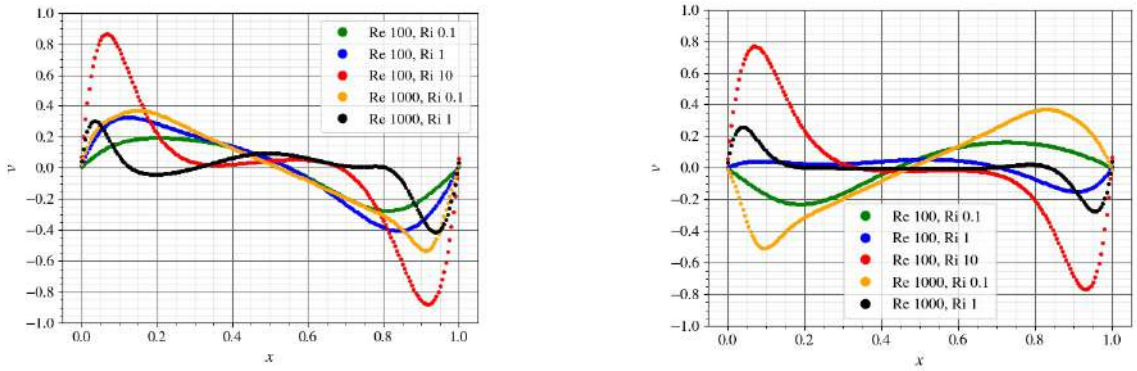

(a) Assisting flow.

(b) Opposing flow.

Figure 10: v-velocity through a horizontal line passing through the geometric center: $AR = 1$.

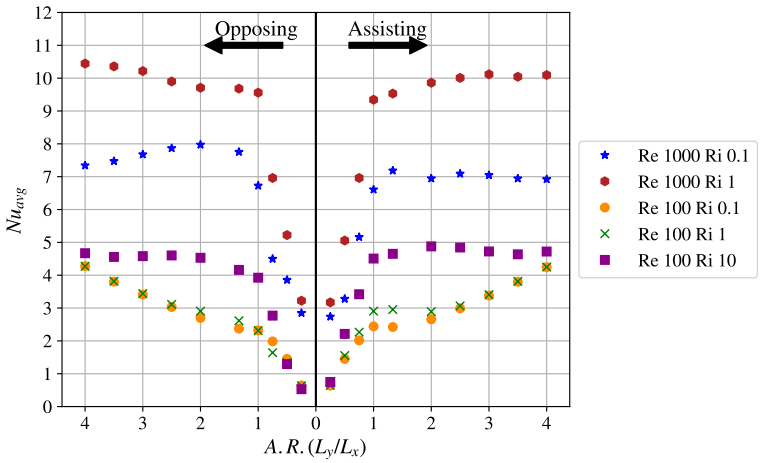

Figure 11: Values of Nu_{avg} for various aspect ratios.

4. CONCLUSIONS

A rectangular cavity with different aspect ratios was analyzed at a mixed convection regime. A small range of Reynolds numbers were used combined to moderate values of Richardson numbers to construe the effects of these parameters on the heat transfer, using the average Nusselt number on the hot wall as a comparative parameter.

A first order explicit finite-difference formulation based on the projection method for the Navier-Stokes equations with Boussinesq approximation was established on the staggered grid. The simulations were made using *Python*, with a 200×200 mesh for all cases.

The results show that for lower values of *Ri* and *AR*, the flow tends to behave according to the shear forces. Higher aspect ratios show for most cases a well established division between two regions, each one dominated by one mechanism. As *Ri* increases, the streamlines suggest that the flow is mainly buoyancy driven. The values of the average Nusselt number however show that the heat transfer is not significantly affected by the direction of the shear forces.

5. REFERENCES

Ameziani, D., Guo, Y., Bennacer, R., El Ganaoui, M. and Bouzidi, M., 2010. "Competition between lid-driven and natural convection in square cavities investigated with a lattice boltzmann method". *Computational Thermal Sciences*, Vol. 2, pp. 269–282.

Barakos, G., Mitsoulis, E. and Assimacopoulos, D., 1994. "Natural convection flow in a square cavity revisited: laminar and turbulent models with wall functions". *International journal for numerical methods in fluids*, Vol. 18, No. 7, pp. 695–719.

Çengel, Y. and Ghajar, A., 2015. *Heat and Mass Transfer: Fundamentals and Applications*. McGraw-Hill Education, New York, 5th edition.

Cheng, T. and Liu, W.H., 2010. "Effect of temperature gradient orientation on the characteristics of mixed convection flow in a lid-driven square cavity". *Computers & Fluids*, Vol. 39, No. 6, pp. 965–978.

Chorin, A.J., 1968. "Numerical solution of the navier-stokes equations". *Mathematics of Computation*, Vol. 22, No. 104, pp. 745–762.

de Vahl Davis, G., 1983. "Natural convection of air in a square cavity: a bench mark numerical solution". *International Journal for numerical methods in fluids*, Vol. 3, No. 3, pp. 249–264.

Fusegi, T., Hyun, J.M. and Kuwahara, K., 1991. "Three-dimensional simulations of natural convection in a sidewall-heated cube". *International Journal for Numerical Methods in Fluids*, Vol. 13, No. 7, pp. 857–867.

Ghia, U., Ghia, K.N. and Shin, C., 1982. "High-Re solutions for incompressible flow using the Navier-Stokes equations and a multigrid method". *Journal of computational physics*, Vol. 48, No. 3, pp. 387–411.

Markatos, N.C. and Pericleous, K., 1984. "Laminar and turbulent natural convection in an enclosed cavity". *International journal of heat and mass transfer*, Vol. 27, No. 5, pp. 755–772.

Oztop, H.F. and Dagtekin, I., 2004. "Mixed convection in two-sided lid-driven differentially heated square cavity". *International Journal of Heat and mass transfer*, Vol. 47, No. 8-9, pp. 1761–1769.

6. RESPONSIBILITY NOTICE

The authors are solely responsible for the printed material included in this paper.